Nuclear Theory'21
ed. V. Nikolaev, Heron Press, Sofia, 2002

Microscopic Treatment of Continuum Effects in Neutron-Rich Nuclei

N. Van Giai

Institut de Physique Nucléaire, Université Paris-Sud, 91406 Orsay Cedex, France

Abstract.

We examine how pairing and continuum effects can be treated self-consistently in the microscopic description of ground states and excited states of neutron-rich nuclei. The starting point is the Hartree-Fock-Bogoliubov (HFB) theory of nuclear ground states. Assuming an effective interaction of the Skyrme type we show how the self-consistent mean field and pairing field can be constructed with the inclusion of the continuum, i.e., with the contributions of HFB states having the correct asymptotic behaviour of scattering waves. We compare the results of continuum-HFB calculations with those of conventional discretized HFB calculations. It is shown that differences are more pronounced in the vicinity of the drip line. On the basis of the continuum-HFB solution one can build the continuum-QRPA approach which provides a consistent description of the excitations. Again, the only input is the effective Skyrme interaction. The continuum-QRPA response function can be calculated. As an illustration, we present and discuss the results obtained for low-lying excitations and giant resonances in neutron-rich Oxygen isotopes.

1 Introduction

Nuclei near drip lines offer challenging problems from the point of view of nuclear structure. First, continuum effects on the bound states are expected to be important because of the small separation energies. Second, such nuclei are not necessarily at closed subshells and therefore, pairing effects must be considered. A peculiarity of pairing correlations in drip line nuclei is their sensitivity to the contribution of continuum single-particle states.

The pairing correlations in the presence of continuum coupling have been treated both in HFB [1–8] and BCS [9–12] approximations. In the HFB approximation the continuum is generally included by solving the HFB equations in coordinate representation. The calculations are done either in the complex energy plane, by using Green functions techniques [1, 6], or on the real energy axes [3, 4]. In the latter case the HFB equations are usually solved by imposing a box boundary condition, i.e., that the HFB wave functions vanish beyond a given distance far from the nucleus. The effect of the resonant continuum upon pairing correlations was studied also in the framework of BCS approximation, both for zero [9–11] and finite temperature [12].

Here, we will show how the HFB equations can be solved by treating the continuum exactly, i.e., with correct boundary conditions. We will also see that the resonant HF-BCS approach can give results very close to those of continuum HFB even in the vicinity of the drip line. A more detailed presentation and discussion can be found in [13].

In nuclei close to the drip lines one expects also a strong connection between the excitations of the system and the properties of the ground state, which may present such specificities as neutron skins. Therefore, in addition to the quasiparticle (qp) spectrum, the residual interaction used in QRPA should be determined from the same two-body force as it is done in the self-consistent continuum RPA calculations [14–16]. In the past years several attempts [17–20] have been made to describe consistently both the pairing correlations and the continuum coupling within QRPA. Here, we present briefly the work of Khan et al. [20] which is the first continuum QRPA calculation with the single-particle spectrum and the residual interaction determined from the same effective two-body force. The ground state is calculated using the continuum HFB approach [13] with the mean field and the pairing field described by a Skyrme interaction and a density-dependent delta force, respectively. Based on the same HFB energy functional we derive the QRPA response function in coordinate space. The QRPA response is constructed by using real energy solutions for the continuum HFB spectrum. The method is illustrated by calculations done for the neutron-rich oxygen isotopes.

2 Continuum HFB

2.1 HFB Equations in Coordinate Representation

The HFB approximation in coordinate representation have been discussed quite extensively in the literature [2–4] and therefore we give here only the basic equations.

The HFB equations in coordinate representation read ([3]):

$$\int d^3\mathbf{r}' \sum_{\sigma'} \begin{pmatrix} h(\mathbf{r}\sigma,\mathbf{r}'\sigma') & \tilde{h}(\mathbf{r}\sigma,\mathbf{r}'\sigma') \\ \tilde{h}(\mathbf{r}\sigma,\mathbf{r}'\sigma') & -h(\mathbf{r}\sigma,\mathbf{r}'\sigma') \end{pmatrix} \begin{pmatrix} \Phi_1(E,\mathbf{r}'\sigma') \\ \Phi_2(E,\mathbf{r}'\sigma') \end{pmatrix} = \begin{pmatrix} E+\lambda & 0 \\ 0 & E-\lambda \end{pmatrix} \begin{pmatrix} \Phi_1(E,\mathbf{r}\sigma) \\ \Phi_2(E,\mathbf{r}\sigma) \end{pmatrix} , \quad (1)$$

where λ is the chemical potential, h and $\tilde{h}$ are the mean field and the pairing field, and Φ_i represents the two-component HFB qp wave function of energy E. The mean field hamiltonian h is a sum of a kinetic energy term T and a mean field term Γ:

$$h(\mathbf{r}\sigma,\mathbf{r}'\sigma') = T(\mathbf{r},\mathbf{r}')\delta_{\sigma\sigma'} + \Gamma(\mathbf{r}\sigma,\mathbf{r}'\sigma') \, . \quad (2)$$

The mean field potential Γ is expressed in terms of the particle-hole two-body interaction V and the particle density ρ in the following way:

$$\Gamma(\mathbf{r}\sigma,\mathbf{r}'\sigma') = \int d^3\mathbf{r_1} d^3\mathbf{r_2} \sum_{\sigma_1\sigma_2} V(\mathbf{r}\sigma,\mathbf{r_1}\sigma_1;\mathbf{r}'\sigma',\mathbf{r_2}\sigma_2)\rho(\mathbf{r_2}\sigma_2,\mathbf{r_1}\sigma_1) \, . \quad (3)$$

In the same way the pairing potential $\tilde{h}$ is expressed in terms of the pairing interaction V_{pair} and the pairing density $\tilde{\rho}$:

$$\tilde{h}(\mathbf{r}\sigma,\mathbf{r}'\sigma') = \int d^3\mathbf{r_1} d^3\mathbf{r_2} \sum_{\sigma_1\sigma_2} 2\sigma'\sigma_2' \times V_{pair}(\mathbf{r}\sigma,\mathbf{r}'-\sigma';\mathbf{r_1}\sigma_1,\mathbf{r_2}-\sigma_2)\tilde{\rho}(\mathbf{r_1}\sigma_1,\mathbf{r_2}\sigma_2) \, . \quad (4)$$

The particle and pairing densities ρ and $\tilde{\rho}$ are defined by the following expressions:

$$\rho(\mathbf{r}\sigma,\mathbf{r}'\sigma') \equiv \sum_{0<E_n<-\lambda} \Phi_2(E_n,\mathbf{r}\sigma)\Phi_2^*(E_n,\mathbf{r}'\sigma') + \int_{-\lambda}^{E_{cut-off}} dE\Phi_2(E,\mathbf{r}\sigma)\Phi_2^*(E,\mathbf{r}'\sigma') \, , \quad (5)$$

$$\tilde{\rho}(\mathbf{r}\sigma,\mathbf{r}'\sigma') \equiv \sum_{0<E_n<-\lambda} \Phi_2(E_n,\mathbf{r}\sigma)\Phi_1^*(E_n,\mathbf{r}'\sigma') + \int_{-\lambda}^{E_{cut-off}} dE\Phi_2(E,\mathbf{r}\sigma)\Phi_1^*(E,\mathbf{r}'\sigma') \, , \quad (6)$$

where the sums are over the bound qp states, with energies $|E| < -\lambda$, and the integral is over the qp continuous states, of energies $|E| > -\lambda$.

The particle-hole and pairing interactions in Eqs.(3) and (4) are chosen as density-dependent contact interactions, so that the integro-differential HFB equations reduce to coupled differential equations. The zero-range character of the

pairing interaction is the reason why one must fix a cut-off in the energy, as it can be seen in Eqs.(5) and (6).

Here, we consider systems with spherical symmetry. In this case the radial and angular components of the HFB wave functions can be introduced [3]:

$$\Phi_i(E, \mathbf{r}\sigma) = u_i(njl, r)\frac{1}{r}y_{lj}^{m_j}(\hat{r}, \sigma) \ , \ i = 1, 2 \ , \tag{7}$$

where

$$y_{lj}^{m_j}(\hat{r}, \sigma) \equiv Y_{lm}(\Theta, \Phi)\chi_{1/2}(m_\sigma)(lm\frac{1}{2}m_\sigma|jm_j) \ . \tag{8}$$

We use for the upper and lower components of the radial wave functions the standard notation $u_{lj}(E, r)$ and $v_{lj}(E, r)$.

2.2 The Treatment of Quasiparticle Continuum

The asymptotic behaviour of the HFB wave function is determined by the physical condition that at large distances the nuclear mean field $\Gamma(r)$ and the pairing field $\Delta(r)$ vanish. This condition requires an effective interaction of finite range. Outside the range of mean fields the equations for $\Phi_i(E, \mathbf{r}\sigma)$ are decoupled and one can easily see how the physical solutions must behave at infinity [2]. Thus, for a negative chemical potential λ, i.e., for a bound system, there are two well separated regions in the qp spectrum. Between 0 and $-\lambda$ the qp spectrum is discrete and both upper and lower components of the radial HFB wave function decay exponentially at infinity:

$$\begin{aligned} u_{lj}(E, r) =& Ah_l^{(+)}(\alpha_1 r) \ , \\ v_{lj}(E, r) =& Bh_l^{(+)}(\beta_1 r) \ , \end{aligned} \tag{9}$$

where $h_l^{(+)}$ are spherical Haenkel functions, $\alpha_1^2 = \frac{2m}{\hbar^2}(\lambda + E)$ and $\beta_1^2 = \frac{2m}{\hbar^2}(\lambda - E)$. These solutions correspond to the bound qp spectrum. For $E > -\lambda$ the spectrum is continuous and the solutions are:

$$\begin{aligned} u_{lj}(E, r) =& C[cos(\delta_{lj})j_l(\alpha_1 r) - sin(\delta_{lj})n_l(\alpha_1 r)] \ , \\ v_{lj}(E, r) =& D_1 h_l^{(+)}(\beta_1 r) \ , \end{aligned} \tag{10}$$

where n_l are spherical Neumann functions and δ_{lj} is the phase shift corresponding to the angular momentum (lj). One can see that the upper component of the HFB wave function has the standard form of a scattering state.

The asymptotic form of the wave function should be matched with the inner radial wave function, which for $r \to 0$ can be written as follows:

$$\begin{pmatrix} u_{lj}(E, r) \\ v_{lj}(E, r) \end{pmatrix} = D_2 \begin{pmatrix} r^{l+1} \\ 0 \end{pmatrix} + D_3 \begin{pmatrix} 0 \\ r^{l+1} \end{pmatrix} \ , \tag{11}$$

The HFB wave function is normalized to the Dirac δ-function of energy. This condition fixes the constant C to the value:

$$C = \sqrt{\frac{1}{\pi}\frac{2m}{\hbar^2\alpha_1}} \, . \tag{12}$$

2.3 Results for Ni Isotopes

We now apply the continuum HFB method to the case of Ni isotopes, which have been investigated extensively both in non-relativistic [5] and relativistic HFB approximation [21, 22].

In the particle-hole channel we use the Skyrme interaction SIII, while in the pairing channel we choose a density-dependent delta interaction:

$$V = V_0 \left[1 - \left(\frac{\rho(r)}{\rho_0}\right)^{\gamma}\right] \, , \tag{13}$$

with the following parameters [5]: $V_0 = 1128.75$, $\rho_0 = 0.134$ and $\gamma = 1$.

As an illustration of continuum effects we show in Figure 1 the occupation probability of the $s1/2$ states in ^{84}Ni for qp energies between $-\lambda$ and 5 MeV. The $s1/2$ continuum exhibits a resonance behaviour peaked at 1.28 MeV. The contributions to pairing from this resonant structure is just the manifestation of the loosely bound $3s1/2$ state.

Let us briefly discuss the predictions given by different approximations: continuum HFB, box-discretized HFB, resonant HF-BCS. The HF-BCS approximation is obtained by neglecting in the HFB equations the non-diagonal matrix elements of the pairing field. This means that in the HF-BCS limit one neglects

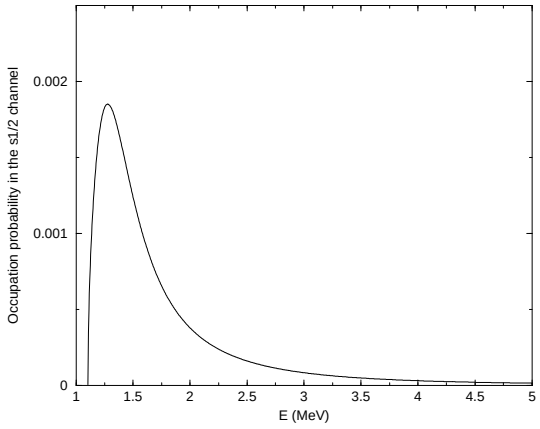

Figure 1. Occupation probability profile in the $s1/2$ channel for ^{84}Ni.

the pairing correlations induced by the pairs formed in states which are not time-reversed partners.

The extension of BCS equations for taking into account the continuum coupling was proposed in Refs. [9,10,12]. For the case of a general pairing interaction the BCS equations reads [10]:

$$\Delta_i = \sum_j V_{i\bar{i}j\bar{j}} u_j v_j + \sum_\nu V_{i\bar{i},\nu\epsilon_\nu\overline{\nu\epsilon_\nu}} \int_{I_\nu} g_\nu(\epsilon) u_\nu(\epsilon) v_\nu(\epsilon) d\epsilon, \tag{14}$$

$$\Delta_\nu \equiv \sum_j V_{\nu\epsilon_\nu\overline{\nu\epsilon_\nu},j\bar{j}} u_j v_j + \sum_{\nu'} V_{\nu\epsilon_\nu\overline{\nu\epsilon_\nu},\nu'\epsilon_{\nu'}\overline{\nu'\epsilon_{\nu'}}} \int_{I_{\nu'}} g_{\nu'}(\epsilon') u_{\nu'}(\epsilon') v_{\nu'}(\epsilon') d\epsilon', \tag{15}$$

$$N = \sum_i v_i^2 + \sum_\nu \int_{I_\nu} g_\nu^c(\epsilon) v_\nu^2(\epsilon) d\epsilon. \tag{16}$$

Here Δ_i are the gaps for the bound states and Δ_ν are the averaged gaps for the resonant states. In these equations the interaction matrix elements are calculated with the scattering wave functions at resonance energies and normalised inside the volume where the pairing interaction is active. The quantity $g_\nu^c(\epsilon) = \frac{2j_\nu+1}{\pi}\frac{d\delta_\nu}{d\epsilon}$ is the total level density and δ_ν is the phase shift of angular momentum $(l_\nu j_\nu)$. The factor $g_\nu^c(\epsilon)$ takes into account the variation of the localisation of scattering states in the energy region of a resonance (i.e., the width effect) and goes to a delta function in the limit of a very narrow width. For more details see Ref. [10].

The two-neutron separation energies S_{2n}:

$$S_{2n} = -B(Z,N) + B(Z,N-2)\ , \tag{17}$$

calculated in various approximations are shown in Figure 2. One can see that in HFB and HF-BCS calculations the change of the sign of the two-neutron separation energies, i.e., the position of the two-neutron dripline, is somewhere between ^{88}Ni and ^{90}Ni, with a faster drop in the case of continuum HFB calculations. The largest differences between HFB and HF calculations appears across the double magic isotope ^{78}Ni. In this case the pairing energy changes fast when two neutrons are removed from $1g9/2$ or added to $2d5/2$. Because the hole state has larger degeneracy than the particle state, the pairing correlations are stronger in ^{76}Ni than in ^{80}Ni. This explains the asymmetry seen in the behaviour of S_{2n} at the crossing of the doubly magic nucleus ^{78}Ni. The fact that the S_{2n} value predicted by HFB for $^{76-78}$Ni are close to the data extrapolated from lighter isotopes indicates that the pairing interaction used in the calculations is quite reasonable, at least for the valence shell $N = 28$-50.

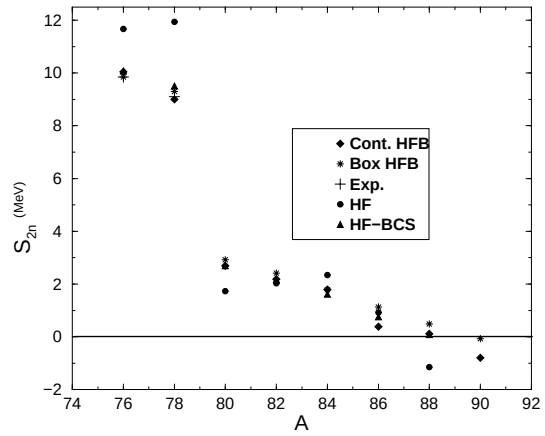

Figure 2. Two-neutron separation energies in HFB, HF-BCS and HF approximations. For ^{76}Ni and ^{78}Ni the corresponding values extrapolated from experimental data are also shown.

The pairing correlation energies are estimated by substracting the binding energies calculated in HFB (or HF-BCS) and HF approach, i.e.,

$$E_p = B(\mathrm{HFB\ or\ HF-BCS}) - B(\mathrm{HF})\ . \tag{18}$$

In Figure 3 we show the pairing correlations energies predicted by HF-BCS approximation in comparison with the continuum HFB results. One can see that the HF-BCS results follow closely the exact HFB values up to the drip line. This shows that for estimating the pairing correlations one needs actually to include from the whole continuum only a few resonant states which should be treated with their width.

3 Continuum QRPA

3.1 Derivation of the Generalized Bethe-Salpeter Equation

The coordinate space formalism is naturally adapted to treat properly the coupling to the continuum states. In Ref. [20] the continuum QRPA equations in coordinate space are obtained as the small amplitude limit of the perturbed time-dependent HFB equations. The main result is that the two-qp Green function satisfies the generalized Bethe-Salpeter equation :

$$\mathbf{G} = (\mathbf{1} - \mathbf{G_0 V})^{-\mathbf{1}}\, \mathbf{G_0} = \mathbf{G_0} + \mathbf{G_0 V G}\ , \tag{19}$$

where $\mathbf{G_0}$ and $\mathbf{V}$ are the unperturbed Green function and the residual qp interaction, respectively.

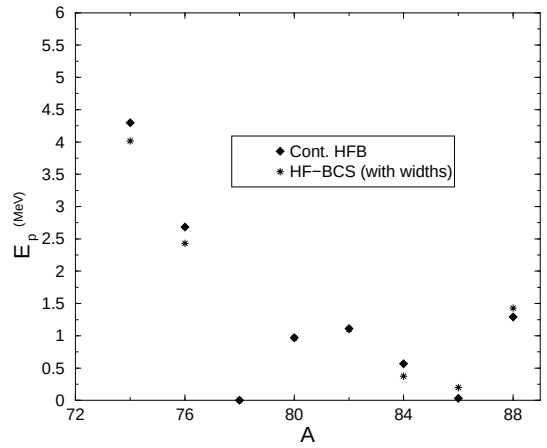

Figure 3. Pairing correlation energies calculated in resonant HF-BCS approximation compared to continuum HFB.

Let us first introduce some notations through the canonical Bogoliubov transformation which relates the particle field operators $\psi^\dagger$ and ψ to the qp operators $\beta^\dagger$ and β:

$$\psi^\dagger(\mathbf{r}\sigma) = \sum_k U_k(\mathbf{r}\sigma)\,\beta_k + V_k^*(\mathbf{r}\sigma)\,\beta_k^\dagger \tag{20}$$

where U_k and V_k are the two components of the HFB wave function of the qp state with energy E_k.

Next, we can define 3-by-2 matrices $\mathcal{U}_{ij}$ by:

$$\mathcal{U}_{ij}(\mathbf{r}\sigma) = \begin{pmatrix} U_i(\mathbf{r}\sigma)V_j(\mathbf{r}\sigma) & U_j^*(\mathbf{r}\sigma)V_i^*(\mathbf{r}\sigma) \\ U_i(\mathbf{r}\sigma)U_j(\mathbf{r}\bar{\sigma}) & V_i^*(\mathbf{r}\sigma)V_j^*(\mathbf{r}\bar{\sigma}) \\ -V_i(\mathbf{r}\sigma)V_j(\mathbf{r}\bar{\sigma}) & -U_i^*(\mathbf{r}\sigma)U_j^*(\mathbf{r}\bar{\sigma}) \end{pmatrix} \tag{21}$$

Here, we have used the notation $f(\mathbf{r}\bar{\sigma})$=$-2\sigma f(\mathbf{r}-\sigma)$ for time-reversed quantities.

Then, the unperturbed Green function $\mathbf{G_0}$ can be expressed as:

$$\mathbf{G_0}^{\alpha\beta}(\mathbf{r}\sigma,\mathbf{r}'\sigma';\omega) = \sum_{ij} -\frac{\mathcal{U}_{ij}^{\alpha 1}(\mathbf{r}\sigma)\bar{\mathcal{U}}_{ij}^{\dagger\beta 1}(\mathbf{r}'\sigma')}{\hbar\omega-(E_i+E_j)+i\eta} + \frac{\mathcal{U}_{ij}^{\alpha 2}(\mathbf{r}\sigma)\bar{\mathcal{U}}_{ij}^{\dagger\beta 2}(\mathbf{r}'\sigma')}{\hbar\omega+(E_i+E_j)+i\eta} \tag{22}$$

where $\bar{\mathcal{U}}_{ij} = \mathcal{U}_{ij} - \mathcal{U}_{ji}$ and α,β = 1,2,3.

The residual interaction matrix $\mathbf{V}$ is:

$$\mathbf{V}^{\alpha\beta}(\mathbf{r}\sigma,\mathbf{r}'\sigma') = \frac{\partial^2\mathcal{E}}{\partial\rho_\beta(\mathbf{r}'\sigma')\partial\rho_{\bar{\alpha}}(\mathbf{r}\sigma)},\ \alpha,\beta = 1,2,3. \tag{23}$$

Here, the notation $\bar{\alpha}$ means that whenever α is 2 or 3 then $\bar{\alpha}$ is 3 or 2.

It should be noted that, in the three dimensional space (α, β), the first dimension represents the particle-hole (ph) subspace, the second the particle-particle (pp) one, and the third the hole-hole (hh) one.

In the case of transitions from the ground state to excited states within the same nucleus, only the (ph,ph) component of $\mathbf{G}$ is acting. If the residual interaction does not depend on spin variables the strength function is thus given by:

$$S(\omega) = -\frac{1}{\pi} Im \int F^{11*}(\mathbf{r}) \mathbf{G}^{11}(\mathbf{r}, \mathbf{r}'; \omega) F^{11}(\mathbf{r}') d\mathbf{r}\, d\mathbf{r}' \tag{24}$$

In the equations above we have not introduced explicitly the isospin degree of freedom. This can be done directly on the final equations by doubling the dimensions of the matrices in order to distinguish between neutrons and protons.

4 HFB+QRPA Calculations of Oxygen Isotopes

4.1 QRPA Calculations

In the QRPA calculations the residual interaction is derived in principle from the interaction used in the HFB, i.e., the Skyrme force and the pairing force (13). The zero-range part of the forces pose no problem. The velocity-dependent termsof the Skyrme force bring additional complications which can be avoided by approximating the residual interaction in the (ph,ph) subspace by its Landau-Migdal limit where the interacting particle and hole have the Fermi momentum and the transferred momentum is zero. The Skyrme interaction has only $l = 0$ and $l = 1$ Landau parameters. Taking the Landau-Migdal form with only $l = 0$ for the (ph,ph) interaction simplifies greatly the numerical task, at the cost of the loss of some consistency. In this work we calculate only natural parity (non spin-flip) excitations and we drop the spin-spin part of the (ph,ph) interaction which plays a minor role. The Coulomb and spin-orbit residual interactions are also dropped.

The QRPA Green function can be evaluated starting with the unperturbed Green function given by Eq.(22). The latter is constructed by using the solutions of the HFB equations, i.e., the qp energies and the corresponding wave functions U and V. All the qp states are included until an energy cutoff of 50 MeV. The generalized Bethe-Salpeter equation (19) is solved with a step of 0.5 fm and all radial integrals are carried out up to 22.5 fm. The strength distribution is calculated until ω_{Max}=50 MeV, with a step of 100 keV and an averaging width η=150 keV. We discuss here two variants of calculations, the full continuum variant and a box variant where the qp spectrum is discretized by calculating the HFB solutions with a box boundary condition, the box radius being 22.5 fm. For ^{24}O only box calculations have been performed.

In a fully consistent calculation the spurious center-of-mass state should come out at zero energy. Because of the Landau-Migdal approximation of the interaction adopted here the consistency between mean field and residual qp interaction is broken and the spurious state becomes imaginary. We cure this defect by renormalizing the residual interaction by a factor α. We find that in all cases the spurious state $J^\pi = 1^-$ comes out at zero energy for α=0.80 . We have checked that the EWSR are satisfied within 1% to 5%.

4.2 Quadrupole Excitations in Oxygen Isotopes

We calculate quadrupole strength distributions with the operators $F_0 = \sum_i r_i^2 Y_{20}(\hat{r_i})$ (isoscalar) and $F_0 = \sum_i r_i^2 Y_{20}(\hat{r_i}) t_z(i)$ (isovector). All results presented correspond to the SLy4 interaction [23]. The strength distributions calculated in the neutron-rich oxygen isotopes are displayed in Figure 4.

One can identify a strong low-lying state and the giant quadrupole resonance (GQR). The low-lying state becomes more isospin-admixed as the neutron excess increases. In the case of ^{24}O the strength distribution is similar to that calculated in Ref. [19] with a Woods-Saxon potential for the mean field although pairing effects are negligible in our calculation whereas the gap Δ of Ref. [19] is sizable. The main difference is the position of the first 2^+ state located at 4.0 MeV here and 5.0 MeV in Ref. [19]. In the other nuclei this low-lying state

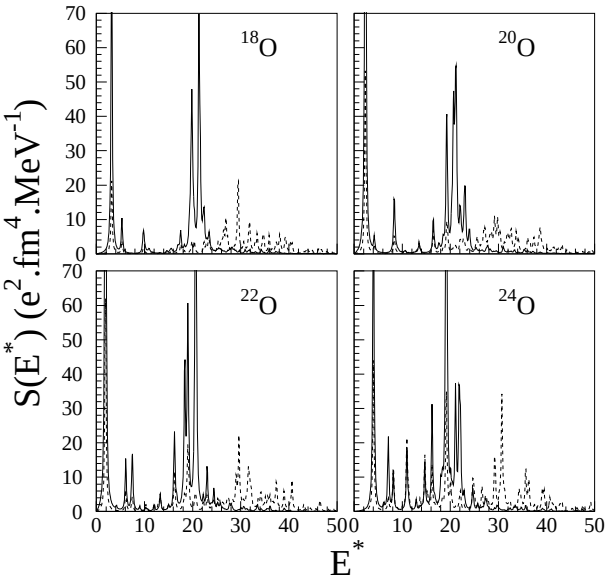

Figure 4. Isoscalar (solid) and isovector (dashed) quadrupole strength functions calculated in continuum-QRPA for the ^{18,20,22,24}O isotopes.

is at lower energies. This is due to the $2s_1/2$ subshell closure in ^{24}O. The HF single-particle energies are given in Table 1. The 2s1/2 state is more bound in the ^{24}O nucleus, suggesting a stronger subshell closure in this case. The occupation factors of these states calculated in HFB are displayed in Table 2. The 2s1/2 starts to be significantly populated in ^{22}O due to the pairing correlations. In the ^{18,20}O spectra mainly 3 low-lying peaks are present. In the unperturbed case they correspond to the (1d5/2,1d5/2), (1d5/2,2s1/2) and (1d5/2,1d3/2) two-qp neutron configurations. Their energies are given in Table 3. In ^{18,20}O the configuration (1d5/2,1d3/2) has a very low strength whereas the (1d5/2,1d5/2), (1d5/2,2s1/2) configurations have similar strength. The effect of the residual interaction, in addition to admix the configurations, is to lower the energy of the initial (1d5/2,1d5/2) peak and to increase the strength of the low-lying state.

Table 1. Single-particle energies (MeV) of the 1d5/2, 2s1/2 and 1d3/2 states in the ^{18,20,22,24}O nuclei calculated with the HF approximation.

	^{18}O	^{20}O	^{22}O	^{24}O
1d5/2	-6.7	-6.9	-7.2	-7.7
2s1/2	-4.0	-4.2	-4.6	-4.9
1d3/2	0.3	0.3	0.2	0.2

Table 2. Occupation factors for the single-qp levels in the ^{18,20,22,24}O nuclei calculated with the HFB model.

	^{18}O	^{20}O	^{22}O	^{24}O
1d5/2	0.31	0.62	0.93	1.
2s1/2	0.03	0.08	0.18	1.
1d3/2	0.01	0.02	0.01	0.

Table 3. Two qp energies (MeV) of the (1d5/2,1d5/2), (1d5/2,2s1/2), and (1d5/2,1d3/2) configurations of the unperturbed strength function for the ^{18,20,22}O nuclei.

	^{18}O	^{20}O	^{22}O
(1d5/2,1d5/2)	4.52	4.16	4.60
(1d5/2,2s1/2)	5.72	4.36	3.35
(1d5/2,1d3/2)	10.39	9.09	2.31

The $E2$ energy and $B(E2)$ value of the first 2^+ state are displayed in Table 4. As noted before, the $E2$ energy in ^{24}O is larger than in other isotopes due to the $2s1/2$ subshell closure. The $E2$ energy in ^{18}O is overestimated and that of ^{22}O is underestimated as compared to experiment. This shows, as noted previously

Table 4. Energy, proton contribution to the reduced transition probabilities B(E2), and ratio of the transition matrix elements M_n/M_p for the first 2^+ state in the ^{18,20,22,24}O nuclei, calculated with the present model. Measured E2, B(E2) values and the M_n/M_p ratios corresponding to the experimental data are displayed in brackets. a) ref. [24]. b) ref. [25]. c) ref. [26]. d) ref. [27]. e) ref. [28].

	^{18}O	^{20}O	^{22}O	^{24}O
$E2$ (MeV)	3.2 (2.0$^{a)}$)	2.3 (1.7$^{a)}$)	1.9 (3.2$^{b)}$)	4.0
B(E2) $(e^2.fm^4)$	14 (45 $\pm$2$^{c)}$)	22 (28 $\pm$2$^{c)}$)	22 (21 $\pm$8$^{d)}$)	9
$(M_n/M_p)_{2^+}$	2.88 (1.10 $\pm$0.24$^{e)}$)	3.36 (3.25$\pm$0.80$^{e)}$)	3.53	4.37

in QRPA calculations with a constant gap ([28]), that the energy prediction of the low-lying modes is a delicate task in RPA-type models. The $B(E2)$ values are well reproduced except for the problematic ^{18}O nucleus. This discrepancy observed for the $B(E2)$ value of ^{18}O is also found in several shell-model calculations [29, 30] and in previous QRPA calculations [28], implying a possible structural anomaly in ^{18}O. Additional investigations in this nucleus are called for. In the case of ^{20,22}O nuclei, the calculated $B(E2)$ are in good agreement with the experimental data. The $B(E2)$ in ^{24}O is predicted smaller than those of lighter isotopes, which supports the $2s_1/2$ subshell closure effect. The calculated M_n/M_p ratios indicate that the neutron are more coherently contributing to the excitation when their number is increasing. For example the M_n/M_p ratio for ^{24}O is more than twice the N/Z value, indicating a very strong neutron contribution to the excitation. The calculated M_n/M_p ratio is correctly reproducing that of ^{20}O deduced from proton scattering experiments. In the case of the experimental M_n/M_p is not well reproduced. This is linked to the fact that the $B(E2)$ value is not well described by the model.

The pairing effects are depicted in Figure 5 where the continuum QRPA calculation is compared to a HF+RPA calculation for the ^{22}O nucleus. The effect of pairing is to shift to higher energy the low-lying peak, and to split the second 2^+ state into two states with smaller strength. There is also some effect in the GQR region.

Box discretization calculations have also been performed in order to test the box boundary condition approximation. The results are shown in Figure 6 for ^{22}O. One can see that only the low-lying state is nearly insensitive whereas the structure of the GQR is more affected by the way the continuum is treated. This shows the necessity of the exact continuum treatment in order to study the giant resonances in neutron-rich oxygen isotopes.

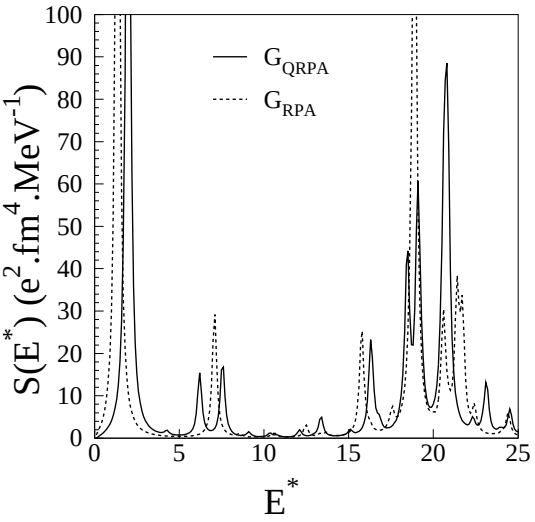

Figure 5. Isoscalar strength function calculated in continuum-QRPA (solid) and HF+RPA (dashed) with box boundary conditions for the ^{22}O nucleus.

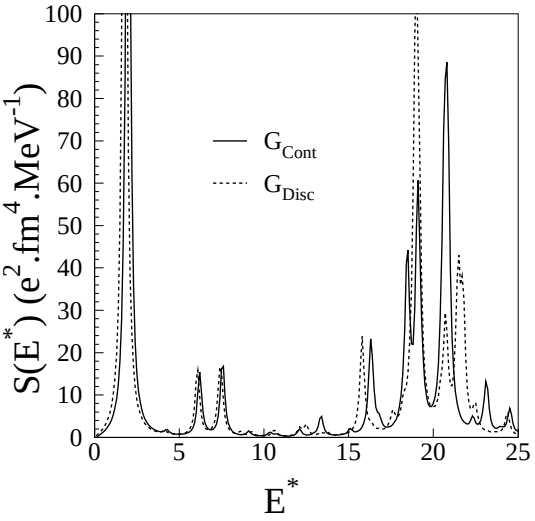

Figure 6. Isoscalar strength function calculated in continuum-QRPA (solid) and with a box discretization (dashed) for the ^{22}O nucleus.

The sensitivity of results with respect to the various Skyrme interactions has been studied. There is no drastic effect coming from the force. The SIII interaction shifts some low-lying states to higher energy and increases the strength of

the state located around 5 MeV. All three interactions produce a splitting of the GQR but the SGII force predicts more strength in the lower component of the giant resonance.

5 Conclusions

In the first part of this paper we have discussed how one can actually solve the HFB equations with proper boundary conditions for the continuous spectrum and we have illustrated the method with applications to neutron-rich Ni isotopes. We have also analyzed how the exact HFB solutions compare to the resonant continuum HF-BCS approximation. It is shown that the resonant HF-BCS calculations that include the first low-lying resonances provide a very good description of pairing correlation energies up to the drip line.

In the second part we have studied the solution of the Bethe-Salpeter equation for the QRPA. Deriving the QRPA as the small amplitude limit of the perturbed time-dependent HFB equations ensures the self-consistency at the conceptual level between the mean field, the pairing field and the qp residual interaction. The QRPA Green function is decomposed into the ph, pp and hh channels. The supermatrix representing the residual interaction is determined self-consistently from the Skyrme and the pairing interactions used in the HFB calculations. As an application we have studied the quadrupole excitations of the neutron-rich oxygen isotopes using Skyrme-type interactions for the mean field and a zero-range, density-dependent interaction for the pairing field. In the numerical study we have approximated the ph residual interaction coming from the Skyrme force by its Landau limit.

The coupling to the continuum appears to have a sizable effect on the GQR and a minor effect on the low-lying states. This shows the importance of the full continuum treatment in order to study giant resonances in neutron-rich nuclei. The low-lying states are sensitive to the pairing interaction. The first 2^+ state of ^{18}O is not well described, as previously noted with other models such as shell-model calculations. Additional investigations on this nucleus are called for. The continuum QRPA shows its ability to reproduce the experimental data of the first 2^+ state for heavier oxygen isotopes., and it predicts a lowering of the $B(E2)$ value for the ^{24}O nucleus. A future improvement of the model will be to include fully the velocity-dependent terms of the Skyrme interaction in the ph channel. Work along these lines is in progress.

Acknowledgments

It is my pleasure to acknowledge the contributions of Marcella Grasso, Elias Khan, Roberto Liotta and Nicu Sandulescu. I thank them for the pleasant collaborations we have had.

References

[1] S.T. Belyaev, A.V. Smirnov, S.V. Tolokonnikov, and S.A. Fayans, (1987) *Sov. J. Nucl. Phys.* **45** 783.

[2] A. Bulgac, (1980) *preprint No. FT-194-1980*, Central Institute of Physics, Bucharest,(*nucl-th/9907088*).

[3] J. Dobaczewski, H. Flocard, and J. Treiner, (1984) *Nucl. Phys.* **A 422** 103.

[4] J. Dobaczewzki, W. Nazarewicz, T.R. Werner, J.-F. Berger, C.R. Chinn, and J. Dechargé, (1996) *Phys. Rev.* **C53** 2809.

[5] J. Terasaki, P.-H. Heenen, H. Flocard, and P. Bonche, (1996) *Nucl. Phys.* **A600** 371.

[6] S.A. Fayans, S.V. Tolokonnikov, and D. Zawischa, (2000) *Phys. Lett.* **B491** 245.

[7] M.V. Stoitsov, W. Nazarewicz, and S. Pittel, (1998) *Phys. Rev.* **C58** 2092.

[8] M.V. Stoitsov, J. Dobaczewski, P. Ring, and S. Pittel, (2000) *Phys. Rev.* **C61** 034311.

[9] N.Sandulescu, R.J.Liotta and R.Wyss, (1997) *Phys. Lett.* **B394** 6.

[10] N.Sandulescu, N.Van Giai and R.J.Liotta, (1997) *Phys. Rev.* **C61** 061301 (R).

[11] A.T.Kruppa, P.H.Heenen and R.J.Liotta, (2001) *Phys. Rev.* **C63** 044324.

[12] N.Sandulescu, O.Civitarese and R.J.Liotta, (2000) *Phys. Rev.* **C 61** 044317.

[13] M. Grasso, N. Sandulescu, N. Van Giai and R.J. Liotta, (2001) *Phys. Rev* **C64** 064321.

[14] G.F.Bertsch and S. F. Tsai, (1975) *Phys. Rep.* **18** 125.

[15] K.F. Liu and N. Van Giai, (1976) *Phys. Lett.* **B 65** 23.

[16] N. Van Giai and H. Sagawa, (1981) *Nucl. Phys* **A371** 1.

[17] S. Kamerdzhiev, R. J. Liotta, E. Litvinova, and V. Tselyaev, (1998) *Phys. Rev* **C64** 172.

[18] K. Hagino and H. Sagawa, (2001) *Nucl. Phys* **A695** 82.

[19] M. Matsuo, (2001) *Nucl. Phys.* **A696** 371.

[20] E. Khan, N. Sandulescu, M. Grasso and N. Van Giai, *nucl-th/0203056*.

[21] J. Meng, (1998) *Phys. Rev.* **C57** 1229.

[22] M. Del Estal, M. Centelles, X. Viñas and S.K. Patra, (2001) *Phys. Rev.* **C63** 044321.

[23] E. Chabanat, P. Bonche, P. Haensel, J. Meyer and R. Schaeffer, (1998) *Nucl. Phys.* **A635** 231.

[24] R. B. Firestone, (1996) *Table of isotopes* Eighth edition.

[25] M. Belleguic *et al., Int. Conf. on Achievements and Perspectives in Nuclear Structure, Crete, Greece, July 99*, to be published in *Physica Scripta*.

[26] S. Raman *et al.*, (1987) *Atomic Data and Nuclear Data Tables* **36** 1.

[27] P. G. Thirolf *et al.*, (2000) *Phys. Lett.* **B485** 16.

[28] E. Khan *et al.*, (2000) *Phys. Lett.* **B490** 45.

[29] B. A. Brown and B. H. Wildenthal, (1988) *Ann. Rev. Part. Nucl. Sci.* **38** 29.

[30] Y. Utsuno, T. Otsuka, T. Mizusaki and M. Honma, (1999) *Phys. Rev* **C60** 054315.